

Ab initio melting temperatures of bcc and hcp iron under the Earth's inner core condition

Yang Sun,^{1,2} Mikhail I. Mendelev,³ Feng Zhang,^{2,4} Xun Liu,⁵ Bo Da,⁵
Cai-Zhuang Wang,^{2,4} Renata M. Wentzcovitch,^{1,6,7} and Kai-Ming Ho²

¹*Department of Applied Physics and Applied Mathematics,
Columbia University, New York, NY 10027, USA*

²*Department of Physics, Iowa State University, Ames, IA 50011, USA*

³*Intelligent Systems Division, NASA Ames Research Center, Moffett Field, CA 94035, USA*

⁴*Ames Laboratory, US Department of Energy, Ames, IA 50011, USA*

⁵*Research and Services Division of Materials Data and Integrated System,
National Institute for Materials Science, Ibaraki 305-0044, Japan.*

⁶*Department of Earth and Environmental Sciences,
Columbia University, New York, NY 10027, USA*

⁷*Lamont-Doherty Earth Observatory, Columbia University, Palisades, NY 10964, USA*

(Dated: May 4, 2022)

There has been a long debate on the thermodynamic stability of iron phases under the Earth's inner core conditions, mainly due to the considerable uncertainty in determining the melting temperatures of iron phases. In the present study, we utilized a semi-empirical potential fitted to high-temperature *ab initio* data to perform a thermodynamic integration from classical systems described by this potential to *ab initio* systems. This method provides a smooth path for the thermodynamic integration and significantly reduces the uncertainty caused by the finite size effect within 15 K. Our results suggest the hcp phase is the ground state of pure iron under the inner core conditions, while the free energy difference between the hcp and bcc phases is tiny, on the order of 10s meV/atom.

Iron is the primary element in the Earth's cores. Its melting temperatures (T_m) under core conditions are essential for understanding the Earth's internal structure and thermal evolution [1]. The solid iron is generally believed to be in the hexagonal close-packed (hcp) structure under the Earth's inner core pressures (323-360 GPa). The body-centered cubic (bcc) structure is also suggested to be stable under core conditions, especially when alloying with light elements at high temperatures [2–7]. The competition between the bcc and hcp polymorphs depends on their Gibbs free energy near T_m . So far, the iron's T_m under Earth's core pressures is poorly constrained. Experimental measurement of this quantity is challenging due to the difficulties in generating the extreme conditions and detecting melts, which has caused different T_m results ranging from 4,850 K to 7,600 K [8]. Most recent experiments provide better constraints but still have an uncertainty of ~ 500 K, which can be even more significant than the difference between the bcc and hcp T_m [9–13]. Besides, differentiation between bcc and hcp iron in high P - T experiments is non-trivial, so bcc iron has rarely been reported at core's pressures and temperature [14].

Computer simulation provides an alternative way to study iron's properties under extreme conditions. Depending on the description of atomic interaction, these simulations can be classified as classical or *ab initio*. The classical simulations utilize semi-empirical potentials to simulate large length-scale atomic structures for a relatively long time. This allows the implementation of

the solid-liquid coexistence (SLC) approach to measure T_m [15]. The SLC approach does not involve any approximations and can determine T_m with inaccuracy not larger than $0.0005 T_m$ [16]. However, the limitation of this method is that the T_m highly depends on the accuracy of the employed semi-empirical potential. On the contrary, *ab initio* simulation provides accurate descriptions of the atomic interaction while it is limited to small lengthscale and timescales, making it almost impossible to utilize the SLC approach.

The free energy approach is the most widely used method to measure the T_m in *ab initio* simulations. It is based on explicit calculations of Gibbs free energies of solid and liquid phases, usually involving thermodynamic integration (TI). TI provides the free energy difference between the target and reference systems for which the absolute free energy is known *a priori*. The harmonic crystal and the ideal gas or simple liquids are popular choices as the reference states for solids and liquids, respectively [17, 18]. While TI provides a decent estimate for absolute free energies, a relatively small inaccuracy in the solid-liquid free energy difference can significantly affect T_m [19]. It was estimated that uncertainty of 10 meV/atom in the free energy difference could lead to uncertainty in T_m of ~ 100 K [20]. Therefore, it is always computationally demanding to calculate T_m accurately using *ab initio* methods. So far, there is only *ab initio* T_m data for hcp Fe [21–23], with the smallest uncertainties still around 200 K [23]. No *ab initio* T_m has been reported for bcc Fe yet. Classical MD reported signifi-

cantly different T_m for bcc at inner core pressures (e.g., 7197 K in [24] and 5974 K in [25]), mainly due to the difference in the employed potentials.

In principle, one does not need the absolute free energy value to calculate T_m . It is the *free energy difference* between the liquid and solid, ΔG^{L-S} , that defines T_m . This quantity can be accurately determined for a classical system (noted as \mathcal{C}) and the corresponding value in *ab initio* system (\mathcal{A}) can be obtained using TI. To realize this approach, one needs a reasonably accurate semi-empirical potential under which the solid phase of interest is at least metastable and a liquid structure is close to the *ab initio* one. Accurate latent heat and the T_m can be obtained from classical MD simulation using the semi-empirical potential with sufficiently large simulation cell and time. These provide the free energy difference between the solid and liquid phases, ΔG_C^{L-S} , associated with melting for the classical system. Then one can perform TI from this classical system to the *ab initio* system to transform the classical ΔG_C^{L-S} into the *ab initio* ΔG_A^{L-S} . The whole process does not involve any approximations, so the computed ΔG_A^{L-S} should be exact. Moreover, since, by design, the classical potential already provides a close description of the solid and liquid phases compared to *ab initio* models, minimal structural changes are expected during the TI. Harmonic and anharmonic contributions are inherently included in the SLC simulations, so this should provide very accurate results. In this study, we develop this approach to compute melting temperatures for the bcc and hcp iron under Earth's inner core pressures.

Formulas.—Assuming the melting temperature T_C^m is known for the classical system, one can compute ΔG_C^{L-S} at T using the Gibbs-Helmholtz equations,

$$\Delta G_C^{L-S}(T) = -T \int_{T_C^m}^T \frac{\Delta H_C}{T^2} dT, \quad (1)$$

where ΔH_C is the latent heat of system \mathcal{C} , which can be directly determined from classical *NPT* MD simulations. The transformation from $\Delta G_C^{L-S}(T)$ to $\Delta G_A^{L-S}(T)$ can be obtained (see Supplementary Materials) as

$$\Delta G_A^{L-S}(T) = \Delta G_C^{L-S}(T) + f_{TI}(T) + f_{PV}(T), \quad (2)$$

where $f_{PV}(T)$ term is the contribution from the equation of state (EoS) difference between \mathcal{A} and \mathcal{C} systems, defined as

$$f_{PV}(T) = [P(V_A^L - V_A^S) - P(V_C^L - V_C^S)] - \left(\int_{V_C^L}^{V_A^L} P_C^L(V) dV - \int_{V_C^S}^{V_A^S} P_C^S(V) dV \right), \quad (3)$$

where V_A^L (or V_A^S) and V_C^L (or V_C^S) are equilibrium volumes of liquid (or solid) at P for system \mathcal{A} and \mathcal{C} , respectively, $P_C^L(V)$ and $P_C^S(V)$ are EoS of liquid and solid for system \mathcal{C} , respectively. $f_{TI}(T)$ term accounts for the TI difference between liquid and solid, which is defined as

$$f_{TI}(T) = \int_0^1 \langle U_A^L - U_C^L \rangle_{\lambda, NVT} d\lambda - \int_0^1 \langle U_A^S - U_C^S \rangle_{\lambda, NVT} d\lambda, \quad (4)$$

where U_A^L (or U_A^S) and U_C^L (or U_C^S) are the internal energy of liquid (or solid) for systems \mathcal{A} and \mathcal{C} , respectively. $\langle \cdot \rangle_{\lambda, NVT}$ is the average in the canonical ensemble with the force field $U = (1 - \lambda) U_A + \lambda U_C$. The subscript *NVT* means the constant conditions of (V_A^L, T) and (V_A^S, T) in liquid and solid simulations, respectively.

$\mathcal{C} \rightarrow \mathcal{C}'$ test.—Eqn.(2) is exact for sufficiently large simulation cells. However, such condition is never satisfied for *ab initio* MD (AIMD) simulations. Since the size and time restrictions of MD simulations are not specific to the type of interatomic interaction (*ab initio* or classical), we can estimate the order of uncertainty by applying the approach to compute the T_m for another classical system \mathcal{C}' where one can test from small to large simulation sizes. In this $\mathcal{C} \rightarrow \mathcal{C}'$ test, the starting system \mathcal{C} is described by the Fe semi-empirical potential developed with embedded atom method (EAM) in [25], where the bcc and hcp T_m have been determined via large-scale SLC simulations as $T_C^m(\text{bcc}) = 5,793$ K and $T_C^m(\text{hcp}) = 5,858$ K at 323 GPa. To build system \mathcal{C}' , we developed another Fe EAM potential (provided in Supplementary Materials) in the same way as [25] except we intentionally changed target T_m . In \mathcal{C}' system, the T_m measured from SLC simulations are $T_{C'}^m(\text{bcc}) = 6,172$ K and $T_{C'}^m(\text{hcp}) = 6,135$ K at 323 GPa. Note the bcc phase has a higher T_m than the hcp phase in the system \mathcal{C}' while it is the opposite in the system \mathcal{C} . The T_m difference between bcc and hcp in the system \mathcal{C}' is within 50 K ($0.008T_m$), which is much smaller than the uncertainty of usual *ab initio* TI using harmonic crystal and simple liquid as references. Therefore, this is a challenging testbed to examine the TI accuracy.

Classical MD simulations were performed using the Large-scale Atomic/Molecular Massively Parallel Simulator (LAMMPS) [26]. The time step of the simulation was 1.0 fs. The Nosé-Hoover thermostat [27] was applied with the damping time $\tau = 0.01$ ps.

To obtain $\Delta G_{C'}^{L-S}$ we first computed ΔG_C^{L-S} using the Gibbs-Helmholtz equation shown in Eqn.(1). The latent heat is obtained from *NPT* MD simulation with $\sim 2,000$ atoms. The results at 323 GPa are shown in Fig. 1(a). To compute the $f_{TI}(T)$ term in Eqn.(4), we performed *NVT* TI-MD with the hybrid Hamiltonian, $H = (1 - \lambda) H_{C'} + \lambda H_C$, where $H_{C'}$ and H_C are the Hamiltonians of \mathcal{C}' and \mathcal{C} systems, respectively. The averaged

internal energy differences between \mathcal{C}' and \mathcal{C} systems are shown as a function of λ in Fig. 1(b), which defines the TI path from \mathcal{C} to \mathcal{C}' . The path is smooth and almost linear, indicating the similarity between two systems. The integrals are computed along the path via Gaussian quadrature. To evaluate the size effect, we compare the TI

path between simulation cells containing 250 and 4,000 atoms. Figure 1(b) shows a systematic deviation between two simulations. This size effect leads to an error of 0.7 meV/atom in the $f_{TI}(T)$. In addition, the error bar of the data from 250-atom simulations is naturally much larger than the ones from 4,000-atom simulations.

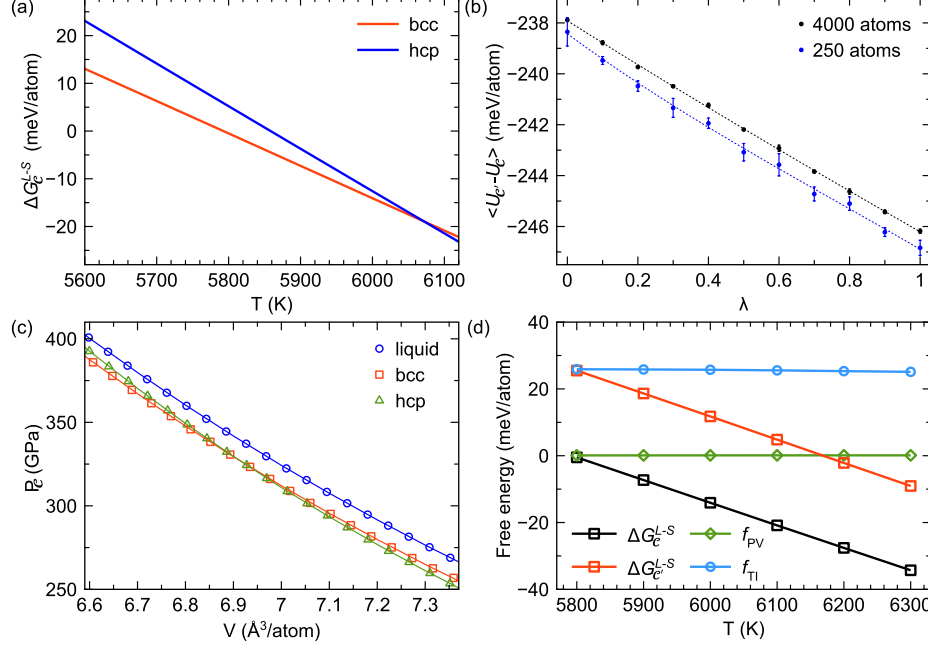


FIG. 1. $\mathcal{C} \rightarrow \mathcal{C}'$ calculations. (a) Gibbs free energy difference between liquid and solid for bcc and hcp as a function of temperature in the system \mathcal{C} at 323 GPa. (b) The TI path from \mathcal{C} to \mathcal{C}' for 250-atom and 4000-atom simulation cells. The error bars are computed by repeating the simulation three times. The dotted line is a polynomial interpolation. (c) EoS of liquid, bcc, and hcp in the system \mathcal{C} at $T = 6,000$ K. The lines are the fitting of third-order Birch-Murnaghan EoS. (d) $\Delta G_{\mathcal{C}'}^{L-S}$ computed from $\Delta G_{\mathcal{C}}^{L-S}$ with the contribution of EoS difference term and TI term, for bcc at 323 GPa using 4,000 atoms. The data points are connected to guide the eyes.

To compute f_{PV} , the first term in Eqn.(3) was directly obtained by measuring the equilibrated volumes of liquids and solids at 323 GPa for systems \mathcal{C}' and \mathcal{C} . The second integral term in Eqn.(3) was obtained by measuring the EoS for system \mathcal{C} . In Fig. 1(c), classical NVT -MD simulations are performed with large simulation cells (4,032 atoms for hcp, 4,394 for bcc, 4,000 for liquid) and a serial of cell volumes to obtain $P_{\mathcal{C}}(V)$ near the pressure of the interest. These results were fitted to the third-order Birch-Murnaghan EoS so that the integral term in Eqn.(3) can be obtained.

Putting $\Delta G_{\mathcal{C}}^{L-S}$, $f_{TI}(T)$, and $f_{PV}(T)$ together via Eqn.(2), we computed the temperature-dependent Gibbs free energy $\Delta G_{\mathcal{C}'}^{L-S}$ for system \mathcal{C}' . The contributions from $f_{TI}(T)$ and $f_{PV}(T)$ are shown in Fig. 1(d). The $f_{PV}(T)$ term is almost zero. The main factor in determining the $\Delta G_{\mathcal{C}'}^{L-S}$ is the $f_{TI}(T)$ term. This term is almost independent of the temperature. The $\Delta G_{\mathcal{C}'}^{L-S}$ for bcc and hcp phases are shown in Fig. 2(a). We obtained $T_{\mathcal{C}'}^m(\text{bcc, TI}) = 6169.1$ K and $T_{\mathcal{C}'}^m(\text{hcp, TI}) = 6131.6$ K. Therefore, we could reproduce the fact that the bcc is

the most stable crystal phase in the system \mathcal{C}' using the TI scheme. Moreover, the obtained values are very close to the T_m measured by the SLC simulations, with the differences of only 3.4 K for hcp and 2.8 K for bcc.

The size effect on the T_m was examined in the $\mathcal{C} \rightarrow \mathcal{C}'$ case by performing the TI simulations using different atom numbers (N_a). Because the limit of simulation size in AIMD only affects the measurement of $f_{TI}(T)$ term, the $\Delta G_{\mathcal{C}}^{L-S}(T)$ and $f_{PV}(T)$ terms are kept the same here. The T_m values calculated from different simulations sizes are shown in Fig. 2(b), together with the T_m data from the SLC simulation for comparison. When the simulation size is larger than 1,000 atoms, the T_m are almost independent on the simulation size and only show a deviation from the SLC results within 5 K. When the simulation size is reduced to ~ 250 atoms, which is the typical cell size of AIMD, the uncertainty in T_m increases to ~ 15 K. This is the consequence of 0.7 meV/atom difference in the $f_{TI}(T)$ between 250-atom and 4000-atom simulations in Fig. 1(b). Compared to the TI calculation using harmonic crystal as the reference, the inaccuracy caused

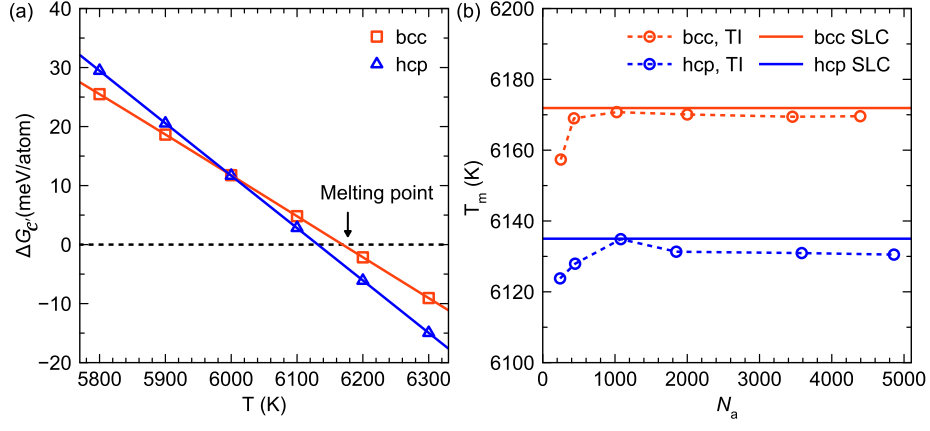


FIG. 2. Melting temperature of C' system and size effect. (a) The Gibbs free energy difference $\Delta G_{C'}^{L-S}$ for bcc and hcp at 323 GPa. The solid line is a polynomial interpolation. The intersection point with the dashed line ($\Delta G_{C'} = 0$) defines T_m . (b) Size effect on TI simulations. The circles are T_m measured from the TI with different numbers of atoms (N_a). The solid line is the T_m from the SLC simulation.

by the size effect is significantly reduced by the current TI scheme. This can be rationalized as follows. The size effect is associated with cutting off longwave phonons in a small simulation cell of crystal phases (the size effect is much less important for liquid models). When TI is performed from a system described by a semi-empirical potential to the *ab initio* system, the effect of the simulation size is only associated with the difference in the phonon distributions between the classical and *ab initio* systems,

which is supposed to be small if the semi-empirical potential was fitted to *ab initio* results. The major contribution of longwave phonons to the free energy difference between the solid and liquid phases is incorporated in reference classical systems via the large-scale SLC simulations. On the contrary, when the TI is performed from a harmonic crystal to the *ab initio* system with a small simulation size, the effect of longwave phonons is ignored because the reference harmonic crystal does not contain the longwave phonon contribution.

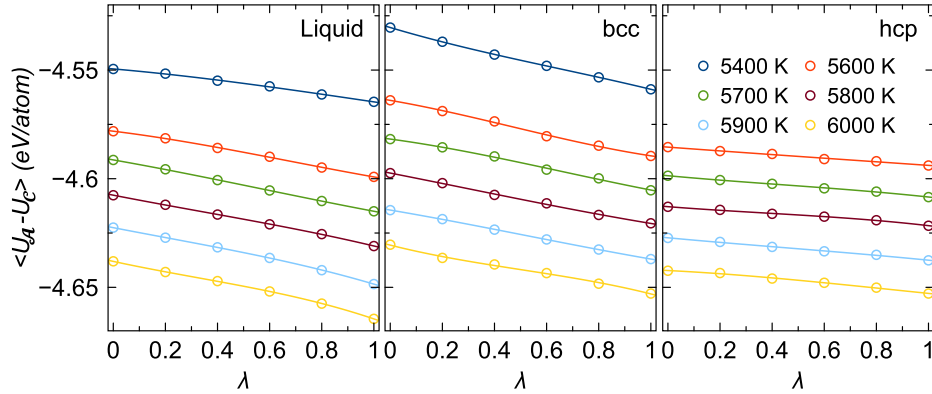


FIG. 3. TI paths of $C \rightarrow A$ at 323 GPa for liquid, bcc, and hcp. The solid lines are polynomial interpolations.

$C \rightarrow A$.—We now compute *ab initio* T_m for hcp and bcc. It requires $\Delta G_C^{L-S}(T)$, $f_{TI}(T)$, and $f_{PV}(T)$ to obtain the $\Delta G_A^{L-S}(T)$ via Eqn.(2). $\Delta G_C^{L-S}(T)$ is the same as the one computed in the $C \rightarrow C'$ case. The $f_{PV}(T)$ terms are computed with the *ab initio* equilibrium volumes of hcp, bcc, and liquid and the classical EoS $P_C(V)$. The main task is to compute the $f_{TI}(T)$ from classical system C to *ab initio* system A .

Ab initio calculations were performed using the Vienna *ab initio* simulation package (VASP) [28]. The projected

augmented-wave method was used and the generalized gradient approximation in the Perdew-Burke-Ernzerhof form was employed for the exchange-correlation energy functional. The electronic entropy was included by the Mermin functional [29, 30] with the electronic temperature same as the ionic temperature. Simulation cells with 240, 250, and 250 atoms were used for hcp, bcc, and liquid, respectively. The Γ point was used to sample the Brillouin zone. In TI-MD simulations, the force acting on each atom was $f = (1 - \lambda)f_A + \lambda f_C$, where f_A and

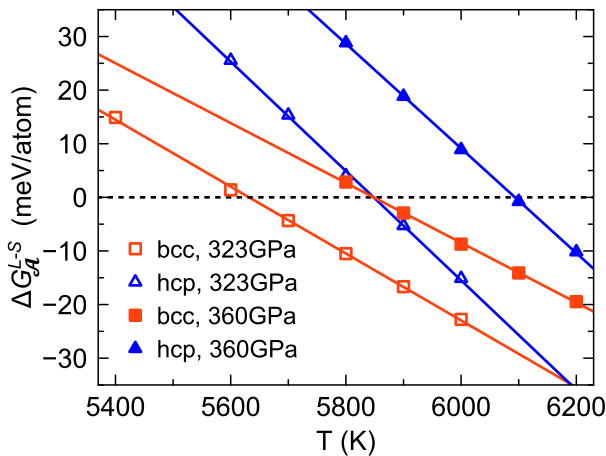


FIG. 4. The *ab initio* Gibbs free energy difference $\Delta G_A^{L-S}(T)$ for bcc and hcp at 323 GPa and 360 GPa. The solid lines are polynomial interpolations. The intersection point with the dashed line defines the T_m .

f_C were the forces generated by *ab initio* calculation and EAM potential, respectively. The *ab initio* forces computed from VASP were passed to LAMMPS on-the-fly with MD simulation. The Nosé-Hoover thermostat [27] was employed to control the temperature. The time step was 2.0 fs.

The *ab initio* TI-MD was performed for liquid, hcp, and bcc in the temperature range from 5,400 K to 6,000 K. The energy differences between *ab initio* system \mathcal{A} and classical system \mathcal{C} , i.e., $\Delta U = \langle U_{\mathcal{A}} - U_{\mathcal{C}} \rangle$, are averaged from TI-MD over 20 ps and shown for three phases in Fig. 3. Just like in the $\mathcal{C} \rightarrow \mathcal{C}'$ case in Fig. 1(b), all the ΔU show smooth and almost linear transitions from classical systems to *ab initio* systems. With these quantities, $\Delta G_A^{L-S}(T)$ and *ab initio* T_m were obtained for both hcp and bcc at 323 GPa and 360 GPa in Fig. 4. The free energy difference between bcc and hcp is very small. At 323 GPa and hcp melting temperature, bcc's free energy is only 14 meV/atom higher than that of hcp.

The current *ab initio* T_m values are shown in Table I. The uncertainty caused by the size effect is estimated as 15 K based on the $\mathcal{C} \rightarrow \mathcal{C}'$ test with similar sizes in Fig. 2(b). According to the present TI calculations, the hcp phase has higher T_m than the bcc phase under both pressures of the inner core boundary and the inner core center. Therefore, the hcp phase should be the ground state for pure Fe at inner-core conditions.

From Table I, the previous *ab initio* TI coupled with phonon quasiparticle method [23] shows for hcp $T_m = 5,730$ K at 330 GPa. This result was obtained using the same pseudopotentials as we used in the *ab initio* TI calculations. Considering the uncertainty of ~ 200 K in previous results [23], our hcp T_m is consistent with it. The T_m data calculated with classical potentials [24, 31] are higher than the present *ab initio* results and are different

TABLE I. The *ab initio* T_m of hcp and bcc from TI calculations at 323 GPa and 360 GPa, and comparison to the data in the literature. The bracket shows the uncertainty.

P/GPa	$T_m(\text{hcp})/\text{K}$	$T_m(\text{bcc})/\text{K}$	Notes
323	5848 (15)	5632 (15)	This work
360	6094 (15)	5850 (15)	This work
330	5730 (200)	-	<i>Ab initio</i> TI + Phonon quasiparticle [23]
360	6838	7197	Classical MD [24]
323	6215	-	Classical MD [31]

from each other. This is expected as different classical potentials can lead to different energy landscapes, and small differences in the free energy can significantly vary T_m .

Conclusions.—We have developed a TI scheme to compute the free energy difference between solid and liquid. This scheme uses the semi-empirical potential as the reference system, providing a smooth TI calculation transition. The T_m of the target system can be computed without calculating the absolute free energy. The test between two classical systems ($\mathcal{C} \rightarrow \mathcal{C}'$) shows that the obtained T_m is very consistent with that from SLC simulations, which provides a good validation for the method. The size effect in the current TI scheme is small, on the order of ~ 15 K difference between 250-atom and 4,000-atom cells. Based on this scheme, the *ab initio* melting temperatures of hcp and bcc iron are calculated at the inner core boundary and the core center pressures. hcp displays a higher T_m than the bcc. Thus, hcp should be the ground state of pure iron at the inner core conditions. However, the free energy difference between the two phases is only on the order of 10s meV/atom. Such a small free energy difference could be easily altered by alloying with other elements, especially if the configurational entropy effect is considered. Future work should include the effect of small amounts of nickel and light elements on the free energy, which is necessary to simulate the inner core.

Work at Iowa State University and Columbia University was supported by the National Science Foundation awards EAR-1918134 and EAR-1918126. We acknowledge the computer resources from the Extreme Science and Engineering Discovery Environment (XSEDE), which is supported by the National Science Foundation grant number ACI-1548562. B. D. is supported by JSPS KAKENHI Grant Number JP21K14656. Molecular dynamics simulations were supported by the Numerical Materials Simulator supercomputer at the National Institute for Materials Science (NIMS).

-
- [1] Y. Zhang and J.-F. Lin, Molten Iron in Earth-like Exoplanet Cores, *Science* (1979) 375, 146 (2022).
- [2] M. Ross, D. A. Young, and R. Grover, Theory of the Iron Phase Diagram at Earth Core Conditions, *Journal of Geophysical Research* 95, 21713 (1990).
- [3] M. Matsui and O. L. Anderson, The Case for a Body-Centered Cubic Phase (α') for Iron at Inner Core Conditions, *Physics of the Earth and Planetary Interiors* 103, 55 (1997).
- [4] L. Vočadlo, D. Alfè, M. J. Gillan, I. G. Wood, J. P. Brodholt, and G. D. Price, Possible Thermal and Chemical Stabilization of Body-Centered-Cubic Iron in the Earth's Core, *Nature* 424, 536 (2003).
- [5] A. B. Belonoshko, T. Lukinov, J. Fu, J. Zhao, S. Davis, and S. I. Simak, Stabilization of Body-Centred Cubic Iron under Inner-Core Conditions, *Nature Geoscience* 10, 312 (2017).
- [6] L. Dubrovinsky et al., Body-Centered Cubic Iron-Nickel Alloy in Earth's Core, *Science* (1979) 316, 1880 (2007).
- [7] K. Kádas, L. Vitos, B. Johansson, and R. Ahuja, Stability of Body-Centered Cubic Iron–Magnesium Alloys in the Earth's Inner Core, *Proceedings of the National Academy of Sciences* 106, 15560 (2009).
- [8] R. A. Fischer, Melting of Fe Alloys and the Thermal Structure of the Core, in *Geophysical Monograph Series* (2016), pp. 1–12.
- [9] R. Sinmyo, K. Hirose, and Y. Ohishi, Melting Curve of Iron to 290 GPa Determined in a Resistance-Heated Diamond-Anvil Cell, *Earth and Planetary Science Letters* 510, 45 (2019).
- [10] J. Li, Q. Wu, J. Li, T. Xue, Y. Tan, X. Zhou, Y. Zhang, Z. Xiong, Z. Gao, and T. Sekine, Shock Melting Curve of Iron: A Consensus on the Temperature at the Earth's Inner Core Boundary, *Geophysical Research Letters* 47, e2020GL087758 (2020).
- [11] S. J. Turneaure, S. M. Sharma, and Y. M. Gupta, Crystal Structure and Melting of Fe Shock Compressed to 273 GPa: In Situ X-Ray Diffraction, *Physical Review Letters* 125, 215702 (2020).
- [12] R. G. Kraus et al., Measuring the Melting Curve of Iron at Super-Earth Core Conditions, *Science* (1979) 375, 202 (2022).
- [13] S. Anzellini, A. Dewaele, M. Mezouar, P. Loubeyre, and G. Morard, Melting of Iron at Earth's Inner Core Boundary Based on Fast X-Ray Diffraction, *Science* (1979) 340, 464 (2013).
- [14] R. Hrubíak, Y. Meng, and G. Shen, Experimental Evidence of a Body Centered Cubic Iron at the Earth's Core Condition, *arXiv* 1804.05109, (2018).
- [15] J. R. Morris and X. Song, The Melting Lines of Model Systems Calculated from Coexistence Simulations, *The Journal of Chemical Physics* 116, 9352 (2002).
- [16] S. R. Wilson, K. G. S. H. Gunawardana, and M. I. Mendelev, Solid-Liquid Interface Free Energies of Pure Bcc Metals and B2 Phases, *Journal of Chemical Physics* 142, 134705 (2015).
- [17] S. Menon, Y. Lysogorskiy, J. Rogal, and R. Drautz, Automated Free-Energy Calculation from Atomistic Simulations, *Physical Review Materials* 5, 103801 (2021).
- [18] R. Freitas, M. Asta, and M. de Koning, Nonequilibrium Free-Energy Calculation of Solids Using LAMMPS, *Computational Materials Science* 112, 333 (2016).
- [19] K. G. S. H. Gunawardana, S. R. Wilson, M. I. Mendelev, and X. Song, Theoretical Calculation of the Melting Curve of Cu-Zr Binary Alloys, *Physical Review E* 90, 052403 (2014).
- [20] D. Alfè, G. D. Price, and M. J. Gillan, Thermodynamics of Hexagonal-Close-Packed Iron under Earth's Core Conditions, *Physical Review B* 64, 045123 (2001).
- [21] D. Alfè, G. D. Price, and M. J. Gillan, Iron under Earth's Core Conditions: Liquid-State Thermodynamics and High-Pressure Melting Curve from *Ab initio* Calculations, *Physical Review B* 65, 165118 (2002).
- [22] E. Sola and D. Alfè, Melting of Iron under Earth's Core Conditions from Diffusion Monte Carlo Free Energy Calculations, *Physical Review Letters* 103, 078501 (2009).
- [23] T. Sun, J. P. Brodholt, Y. Li, and L. Vočadlo, Melting Properties from *Ab initio* Free Energy Calculations: Iron at the Earth's Inner-Core Boundary, *Physical Review B* 98, 224301 (2018).
- [24] A. B. Belonoshko, J. Fu, and G. Smirnov, Free Energies of Iron Phases at High Pressure and Temperature: Molecular Dynamics Study, *Physical Review B* 104, 104103 (2021).
- [25] Y. Sun, F. Zhang, M. I. Mendelev, R. M. Wentzcovitch, and K.-M. Ho, Two-Step Nucleation of the Earth's Inner Core, *Proceedings of the National Academy of Sciences* 119, e2113059119 (2022).
- [26] A. P. Thompson et al., LAMMPS - a Flexible Simulation Tool for Particle-Based Materials Modeling at the Atomic, Meso, and Continuum Scales, *Computer Physics Communications* 271, 108171 (2022).
- [27] S. Nosé, A Unified Formulation of the Constant Temperature Molecular Dynamics Methods, *The Journal of Chemical Physics* 81, 511 (1984).
- [28] G. Kresse and J. Furthmüller, Efficient Iterative Schemes for *Ab initio* Total-Energy Calculations Using a Plane-Wave Basis Set, *Physical Review B* 54, 11169 (1996).
- [29] N. D. Mermin, Thermal Properties of the Inhomogeneous Electron Gas, *Physical Review* 137, A1441 (1965).
- [30] R. M. Wentzcovitch, J. L. Martins, and P. B. Allen, Energy versus Free-Energy Conservation in First-Principles Molecular Dynamics, *Physical Review B* 45, 11372 (1992).
- [31] C. J. Davies, M. Pozzo, and D. Alfè, Assessing the Inner Core Nucleation Paradox with Atomic-Scale Simulations, *Earth and Planetary Science Letters* 507, 1 (2019).

Supplemental Material for “*Ab initio* melting temperatures of bcc and hcp iron under the Earth’s inner core condition”

In this Supplemental Material we provide the derivation of formulas transforming classical T_m and solid-liquid free energy difference to *ab initio* ones.

Let’s consider two systems \mathcal{A} and \mathcal{C} , which are described by *ab initio* and classical force fields, respectively. We assume the melting temperature T_m^m are known for the classical system (calculated by large solid-liquid coexistence simulations in practice). In the following, we derive the equation to obtain the free energy difference and T_m for system \mathcal{A} , i.e. $\Delta G_{\mathcal{A}}^{L-S}$ and T_m^m . We start from the definition:

$$\Delta G_{\mathcal{A}}^{L-S}(T) = F_{\mathcal{A}}^L(V_{\mathcal{A}}^L, T) - F_{\mathcal{A}}^S(V_{\mathcal{A}}^S, T) + P(V_{\mathcal{A}}^L - V_{\mathcal{A}}^S), \quad (\text{S1})$$

where P and T are pressure and temperature, $V_{\mathcal{A}}^L$ and $V_{\mathcal{A}}^S$ are equilibrium volumes and $F_{\mathcal{A}}^L(T)$ and $F_{\mathcal{A}}^S(T)$ are Helmholtz free energies of liquid and solid in system \mathcal{A} at (P, T) , respectively. Performing the thermodynamics integration (TI) from the classical system \mathcal{C} for liquid and solid, one can compute the Helmholtz free energies as

$$\begin{aligned} F_{\mathcal{A}}^L(V_{\mathcal{A}}^L, T) - F_{\mathcal{C}}^L(V_{\mathcal{A}}^L, T) &= \int_0^1 \langle U_{\mathcal{A}}^L - U_{\mathcal{C}}^L \rangle_{\lambda, NVT} d\lambda \\ F_{\mathcal{A}}^S(V_{\mathcal{A}}^S, T) - F_{\mathcal{C}}^S(V_{\mathcal{A}}^S, T) &= \int_0^1 \langle U_{\mathcal{A}}^S - U_{\mathcal{C}}^S \rangle_{\lambda, NVT} d\lambda, \end{aligned} \quad (\text{S2})$$

where $\langle \cdot \rangle_{\lambda, NVT}$ is the ensemble average of internal energy over configurations sampled in the canonical ensemble with the force field $U = (1 - \lambda)U_{\mathcal{A}} + \lambda U_{\mathcal{C}}$. The subscript NVT means the constant conditions of $(V_{\mathcal{A}}^L, T)$ and $(V_{\mathcal{A}}^S, T)$ in liquid and solid simulations, respectively. We note the *ab initio* internal energy, $U_{\mathcal{A}}$, includes the electronic entropy contribution. For simplicity’s sake, we denote the integral terms in Eqn.(S2) as $F_{TI}^L(V_{\mathcal{A}}^L, T) = \int_0^1 \langle U_{\mathcal{A}}^L - U_{\mathcal{C}}^L \rangle_{\lambda, NVT} d\lambda$ and $F_{TI}^S(V_{\mathcal{A}}^S, T) = \int_0^1 \langle U_{\mathcal{A}}^S - U_{\mathcal{C}}^S \rangle_{\lambda, NVT} d\lambda$. Then Eqn.(S2) can be rewritten as

$$F_{\mathcal{A}}^L(V_{\mathcal{A}}^L, T) - F_{\mathcal{A}}^S(V_{\mathcal{A}}^S, T) = F_{TI}^L(V_{\mathcal{A}}^L, T) - F_{TI}^S(V_{\mathcal{A}}^S, T) + F_{\mathcal{C}}^L(V_{\mathcal{A}}^L, T) - F_{\mathcal{C}}^S(V_{\mathcal{A}}^S, T). \quad (\text{S3})$$

The last two terms in Eqn.(S3) require the free energy of the classical system \mathcal{C} . Given the calculated melting temperature T_m^m , one can accurately compute the Gibbs free energy difference between liquid and solid $\Delta G_{\mathcal{C}}^{L-S}$ at T using the Gibbs-Helmholtz equations,

$$\Delta G_{\mathcal{C}}^{L-S}(T) = -T \int_{T_m^m}^T \frac{\Delta H_{\mathcal{C}}}{T^2} dT, \quad (\text{S4})$$

where $\Delta H_{\mathcal{C}}$ is the latent heat of system \mathcal{C} , which can be directly determined from classical NPT MD simulations. As $\Delta G_{\mathcal{C}}^{L-S}(T) = G_{\mathcal{C}}^L(T) - G_{\mathcal{C}}^S(T)$, one can write it as

$$\Delta G_{\mathcal{C}}^{L-S}(T) = F_{\mathcal{C}}^L(V_{\mathcal{C}}^L, T) - F_{\mathcal{C}}^S(V_{\mathcal{C}}^S, T) + P(V_{\mathcal{C}}^L - V_{\mathcal{C}}^S), \quad (\text{S5})$$

where $V_{\mathcal{C}}^L$ and $V_{\mathcal{C}}^S$ are the equilibrium volumes of classical liquid and solid under the condition of (P, T) . Note $V_{\mathcal{C}}^L$ and $V_{\mathcal{C}}^S$ are not necessarily the same as $V_{\mathcal{A}}^L$ and $V_{\mathcal{A}}^S$ owing to the difference between classical and *ab initio* force fields. Since $P = -\frac{\partial F}{\partial V}|_T$, we can write

$$\begin{aligned} F_{\mathcal{C}}^L(V_{\mathcal{A}}^L, T) - F_{\mathcal{C}}^L(V_{\mathcal{C}}^L, T) &= - \int_{V_{\mathcal{C}}^L}^{V_{\mathcal{A}}^L} P_{\mathcal{C}}^L(V) dV \\ F_{\mathcal{C}}^S(V_{\mathcal{A}}^S, T) - F_{\mathcal{C}}^S(V_{\mathcal{C}}^S, T) &= - \int_{V_{\mathcal{C}}^S}^{V_{\mathcal{A}}^S} P_{\mathcal{C}}^S(V) dV, \end{aligned} \quad (\text{S6})$$

where $P_{\mathcal{C}}^L(V)$ and $P_{\mathcal{C}}^S(V)$ are the equation of states of liquid and solid in the classical system at T . Combining both Eqns.(S6) we obtain

$$F_{\mathcal{C}}^L(V_{\mathcal{A}}^L, T) - F_{\mathcal{C}}^S(V_{\mathcal{A}}^S, T) = F_{\mathcal{C}}^L(V_{\mathcal{C}}^L, T) - F_{\mathcal{C}}^S(V_{\mathcal{C}}^S, T) - \left(\int_{V_{\mathcal{C}}^L}^{V_{\mathcal{A}}^L} P_{\mathcal{C}}^L(V) dV - \int_{V_{\mathcal{C}}^S}^{V_{\mathcal{A}}^S} P_{\mathcal{C}}^S(V) dV \right). \quad (\text{S7})$$

Now combining Eqns.(S3), (S5), and (S7), we can write Eqn.(S1) as

$$\Delta G_{\mathcal{A}}^{L-S}(T) = \Delta G_{\mathcal{C}}^{L-S}(T) + F_{TI}^L(V_{\mathcal{A}}^L, T) - F_{TI}^S(V_{\mathcal{A}}^S, T) + [P_0(V_{\mathcal{A}}^L - V_{\mathcal{A}}^S) - P_0(V_{\mathcal{C}}^L - V_{\mathcal{C}}^S)] - \left(\int_{V_{\mathcal{C}}^L}^{V_{\mathcal{A}}^L} P_{\mathcal{C}}^L(V) dV - \int_{V_{\mathcal{C}}^S}^{V_{\mathcal{A}}^S} P_{\mathcal{C}}^S(V) dV \right). \quad (\text{S8})$$

We define the TI term $f_{TI}(T)$ and the PV difference term $f_{PV}(T)$ as

$$f_{TI}(T) = F_{TI}^L(V_{\mathcal{A}}^L, T) - F_{TI}^S(V_{\mathcal{A}}^S, T), \quad (\text{S9})$$

$$f_{PV}(T) = [P(V_{\mathcal{A}}^L - V_{\mathcal{A}}^S) - P(V_{\mathcal{C}}^L - V_{\mathcal{C}}^S)] - \left(\int_{V_{\mathcal{C}}^L}^{V_{\mathcal{A}}^L} P_{\mathcal{C}}^L(V) dV - \int_{V_{\mathcal{C}}^S}^{V_{\mathcal{A}}^S} P_{\mathcal{C}}^S(V) dV \right). \quad (\text{S10})$$

Now Eqn.(S8) can be simplified as

$$\Delta G_{\mathcal{A}}^{L-S}(T) = \Delta G_{\mathcal{C}}^{L-S}(T) + f_{TI}(T) + f_{PV}(T). \quad (\text{S11})$$

Using $\Delta G_{\mathcal{A}}^{L-S}(T)$ one can compute the melting temperature under the condition of $\Delta G_{\mathcal{A}}^{L-S}(T_{\mathcal{A}}^m) = 0$. To this end, the $f_{TI}(T)$ term requires TI simulation from system \mathcal{C} to system \mathcal{A} . The $f_{PV}(T)$ term requires equilibrium volume $V_{\mathcal{A}}^L$ and $V_{\mathcal{A}}^S$ at P for system \mathcal{A} and equation of state $P_{\mathcal{C}}^L(V)$ and $P_{\mathcal{C}}^S(V)$, which can all be directly computed from *ab initio* and classical MD simulations.
